

Measurements of Ambipolar Seebeck Coefficients in High-Mobility Diketopyrrolopyrrole Donor–Acceptor Copolymers

Katharina Broch,^{*} Deepak Venkateshvaran,^{*} Vincent Lemaure, Yoann Olivier, David Beljonne, Mateusz Zelazny, Iyad Nasrallah, David J. Harkin, Martin Statz, Riccardo Di Pietro, Auke Jisk Kronemeijer, and Henning Sirringhaus

The Seebeck coefficient of both electrons and holes in a family of ambipolar diketopyrrolopyrrole copolymers is investigated using field-effect gated measurements. It is found that at high carrier concentrations the magnitude of the Seebeck coefficients is not strongly dependent on the molecular structure of the backbone within this family of polymers. Additionally, the Seebeck coefficients of electrons and holes have very similar magnitudes showing that electrons and holes experience a similar energetic landscape. Subtle differences in the carrier concentration dependence between the polymers are observed, which are interpreted in terms of different degrees of energetic disorder on the basis of molecular dynamics and electronic structure simulations.

of a thermoelectric material can be assessed in terms of its figure of merit $ZT = \alpha^2 \sigma T / \kappa$, which governs the dependence of the efficiency of a thermoelectric converter on material properties.^[3–6] Here, α represents the Seebeck coefficient, σ the electrical conductivity, and κ the thermal conductivity. $ZT = 1$ is considered a useful performance threshold required for many applications.^[7,8] Inorganic materials systems used today in the conversion of vehicular exhaust heat in automobiles are based on BiTe and its alloys and exhibit $ZT = 1$ at relatively high temperatures between 400 and 600 K.^[7,9,10] Another

1. Introduction

Organic-conjugated polymers and molecules are being researched for a range of thin-film electronic and optoelectronic applications, including thermoelectric converters that convert waste heat into utilizable electrical energy.^[1,2] The performance

of an inorganic alloy in commercial use in radioisotope thermoelectric generators to power space probes for deep space exploration is SiGe which achieves $ZT = 1$ at an even higher temperature of 900 K.^[7] In comparison, the highest reported value of ZT in an organic polymer was recently measured in poly(3,4-ethylenedioxythiophene):polystyrene sulfonate (PEDOT:PSS) where it was shown to be 0.42 at 300 K.^[11] PEDOT:PSS has been the material of choice for organic thermoelectrics to date.^[12,13]

For applications in light-emitting diodes, solar cells, and field-effect transistors, the performance of organic semiconductors has increased dramatically as a result of an intense effort in molecular optimization over the last 20–30 years. It appears likely that the thermoelectric properties of organic semiconductors could also be improved significantly through molecular design and tuning by chemical synthesis. However, at present the basic molecular-structure-thermoelectric-property relationships remain comparatively poorly understood. In particular, the relationship between the magnitude of the Seebeck coefficient and the molecular and thin-film microstructure should be explored in more depth and in a wider range of materials' systems, in particular, systems with high charge carrier mobilities, that are likely to be of most interest for thermoelectric applications.

High-mobility ambipolar copolymers have attracted considerable interest owing to their use in state-of-the-art organic field-effect transistor (FET) devices. These narrow bandgap ambipolar copolymers exhibit electron and hole mobilities on the order of $1 \text{ cm}^2 \text{ V}^{-1} \text{ s}^{-1}$, and open up new pathways to implement organic electronic architectures with a CMOS-like functionality.^[14–16] Many of these polymers have not yet been

Dr. K. Broch,^[†] Dr. D. Venkateshvaran, Dr. I. Nasrallah, M. Zelazny, Dr. D. J. Harkin, M. Statz, Prof. H. Sirringhaus
 Optoelectronics Group
 Cavendish Laboratory
 University of Cambridge
 JJ Thomson Avenue
 Cambridge CB3 0HE, UK
 E-mail: katharina-anna.broch@uni-tuebingen.de; dv246@cam.ac.uk

Dr. V. Lemaure, Dr. Y. Olivier, Dr. D. Beljonne
 Laboratory for Chemistry of Novel Materials
 Université de Mons
 20 Place du Parc, Mons 7000, Belgium

Dr. R. Di Pietro
 Hitachi Cambridge Laboratory
 J. J. Thomson Avenue
 Cambridge CB3 0HE, UK

Dr. A. J. Kronemeijer
 TNO/Holst Centre
 High Tech Campus 31, 5656 AE Eindhoven, Netherlands

^[†]Present address: Institut für Angewandte Physik, Universität Tübingen, Auf der Morgenstelle 10, 72076 Tübingen, Germany

The ORCID identification number(s) for the author(s) of this article can be found under <https://doi.org/10.1002/aelm.201700225>.

DOI: 10.1002/aelm.201700225

studied in heat-gradient-driven, thermoelectric device architectures.^[17–22] A powerful and convenient method to study the Seebeck coefficient is to perform Seebeck measurements in an FET architecture. Although practical thermoelectric converters rely mainly on the use of bulk-doped thermoelectric materials, such field-effect-gated Seebeck measurements allow relatively straightforward assessment of the Seebeck coefficient of a material without the complexities associated with chemical doping and provide powerful insight into the physics of carrier transport and disorder in organic semiconductors. They allow assessment of the Seebeck coefficient at a well-defined carrier concentration (defined by the applied gate voltage). In bulk-doped polymers, it is often not straightforward to determine the carrier concentration, as Hall effect measurements are not always possible or are difficult to interpret, and the doping efficiency for a specific dopant is also highly dependent on the polymer system. This makes it difficult to establish relationships between molecular structure and the Seebeck coefficient. In gated Seebeck measurements, such comparisons between different materials should be more straightforward.

Gated Seebeck measurements should be particularly interesting for conjugated polymers with ambipolar transport properties as they might also allow comparing the Seebeck coefficients of electron and hole charge carriers, which is important because thermoelectric converters require both n-type and p-type devices. In bulk-doped samples, investigation of the electron–hole symmetry of the Seebeck coefficient is challenging as in many materials systems efficient doping can only be achieved for either holes or electrons depending on the energy levels of the polymer. In contrast, in an ambipolar FET the charge transport can be switched from p-type to n-type simply by reversing the polarity of the gate voltage. In this work, the simultaneous measurement of the Seebeck coefficients for holes and electrons within an FET depending on the accumulated carrier type in the channel is demonstrated for the first time. The Seebeck coefficient is a thermoelectric transport coefficient that represents the entropy transported per unit charge carrier in a material.^[3,23] A measurement of the gate-voltage-modulated Seebeck coefficient has been shown to be a sensitive probe of energetic disorder within the conjugated polymer.^[18] These measurements therefore provide a sensitive probe of the energetic landscape that electron and hole carriers experience as they travel along the channel at the interface.

The organic semiconductors investigated in this work comprise four high-mobility donor–acceptor copolymers based on diketopyrrolopyrrole (DPP) that are copolymerized with varying molecular motifs such as thienothiophene (DPP-DTT), thiophene (DPP-TTT), diselenophene-benzothiadiazole (SeDPP-BT), and benzotriazole (DPP-BTz) (**Figure 1a**).^[14,15,24,25] When integrated into a standard top-gate polymer FET architecture, all these polymers show characteristic ambipolar transfer curves with either hole or electron currents in the channel depending on the polarity of gate voltage applied. These ambipolar copolymers are investigated here by carrier-modulated electrical and thermoelectric measurements as well as numerical simulations of polymer microstructure and the associated energetic broadening of the density of states. Our aim is to relate differences in the magnitude and carrier concentration of the Seebeck coefficient of electrons and holes to the polymer structure and

microstructure and in this way begin to understand to which extent the Seebeck coefficient is influenced by polymer design, chain conformation, and packing.

2. Results

The architecture for the electrical and thermoelectric measurements used in this work is shown in **Figure 1b**. It consists of a conventional bottom-contact, top-gate transistor architecture with a PMMA gate dielectric and a micropatterned heater next to one of the electrodes. This micropatterned heater is necessary for gate-voltage-modulated Seebeck measurements to create an in-plane temperature gradient between the two electrodes in response to which a thermal voltage is generated.^[17] In the current work, a four-point probe resistance to temperature calibration on each of the sensors (source drain electrodes) is used (as opposed to a two-point probe measurement used previously) for enhanced accuracy in the estimation of the temperature gradient. The Seebeck coefficient is extracted as a linear fit to a plot of measured thermal voltage versus applied temperature difference at various gate biases. In the absence of on-chip heating using the micropatterned heater, the device performs as a transistor with a source, drain, and gate electrode. The transistor transfer curves of the four different polymers studied herein are shown in **Figure 2**. All devices show clean ambipolar characteristics with electron accumulation for positive gate voltages and hole accumulation for negative gate voltages. The gate leakage current is several orders of magnitude lower than the transistor current. **Table 1** shows a summary of the mobility values which we have measured on these polymers in optimized FET structures with unpatterned semiconductor layers but with the same gate dielectric and using robust mobility extraction methods. In the gated Seebeck architecture, the need for patterning of the active semiconductor caused a small reduction in the transistor ON currents, presumably due to degradation of the polymer during the photolithographic patterning process.

The experimentally determined Seebeck coefficient α is shown in **Figure 3** as a function of the applied gate voltage V_G (**Figure 3a**) and as a function of the charge carrier density n (**Figure 3b**). The charge carrier density was calculated from the measured gate dielectric capacitance assuming a 1 nm thickness of the accumulation layer. For comparison, the carrier-modulated Seebeck coefficient of indacenodithiophene-*co*-benzothiadiazole (IDTBT), a conjugated polymer with very low degree of torsional disorder,^[18] is also shown. For the IDTBT device, we used a Cytop gate dielectric (because IDTBT is somewhat soluble in the solvents that can be used for deposition of PMMA). As a result, the accessible carrier concentrations in the IDTBT reference devices are lower due to the smaller dielectric constant of Cytop compared to PMMA and we were only able to observe unipolar hole transport, as Cytop does not allow observation of electron accumulation in IDTBT. For all four DPP polymers, we were able to measure clean positive and negative Seebeck signals over a range of negative and positive gate voltages, which is allowing us to compare the magnitude and carrier concentration dependence of the Seebeck coefficient of electrons and holes.

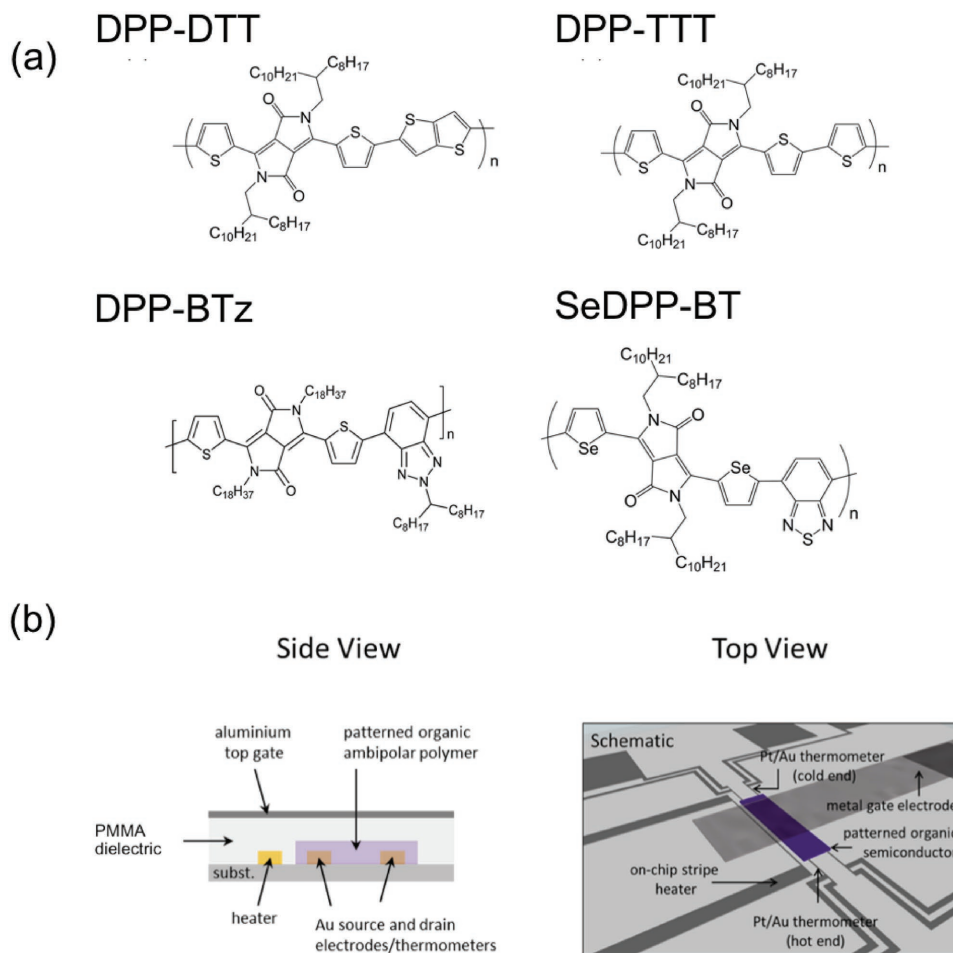


Figure 1. a) Chemical structures of DPP-DTT, DPP-TTT, DPP-BTz, and SeDPP-BT. b) Schematic diagrams of the device geometry for transistor and Seebeck measurements.

The most striking observation in Figure 3 is that at high carrier concentrations the magnitudes of the Seebeck coefficients of all the DPP copolymers are very similar. The values of the Seebeck coefficient at a carrier concentration of 10^{19} cm^{-3} and the slope of $\frac{d\alpha}{d \log n}$ are summarized for the five polymers in **Table 2**. The average values are on the order of $366 \mu\text{V K}^{-1}$ for holes and $395 \mu\text{V K}^{-1}$ for electrons with standard deviations of only 43 and $78 \mu\text{V K}^{-1}$. This suggests that differences in molecular structure and microstructure within this family of polymers only have relatively minor influence on the magnitude of the Seebeck coefficient. This is not too surprising as in the high carrier concentration regime most shallow trap states within the polymer will have been filled and the Seebeck coefficient is determined only by the concentration of gate-induced charges and the density of thermally accessible sites on the polymer. We have previously argued^[18] that in a high charge carrier concentration regime where charge trapping can be neglected, the Seebeck coefficient can be approximated by Heikes formula

$$\alpha = \frac{k_B}{e} \ln\left(\frac{N-n}{n}\right) + \frac{k_B}{e} \ln 2 \quad (1)$$

Here, N is the density of thermally accessible sites. This predicts a value of $198 \mu\text{V K}^{-1}$ for the slope $\frac{d\alpha}{d \log n}$. Among the DPP polymers the Seebeck values for holes in DPP-BTz and DPP-TTT and the value for electrons in Se-DPP-BT come to within 40% of this ideal value, almost as close as for IDTBT, which is the conjugated polymer with the lowest degree of energetic disorder discovered so far.^[18] By fitting the Seebeck coefficients of our DPP copolymers at high carrier concentration to Heikes formula (Equation (1)) we can extract typical values of $N = 5 \times 10^{20} \text{ cm}^{-3}$ for the density of thermally accessible sites in our DPP copolymers. If we assume that the density of thermally accessible sites is determined by the length of the polymer repeat unit and the typical interchain packing density, it may not be too surprising that the Seebeck coefficient of the four polymers is similar at high gate voltages as all polymers have similar repeat unit lengths and packing density. This is somewhat higher than the value found in our reference polymer IDTBT ($N = 0.6 \times 10^{20} \text{ cm}^{-3}$), which exhibits a relatively smaller Seebeck coefficient at the same carrier concentration. This observation potentially reflects the long, branched side chain substitution of IDTBT that prevents close interchain stacking

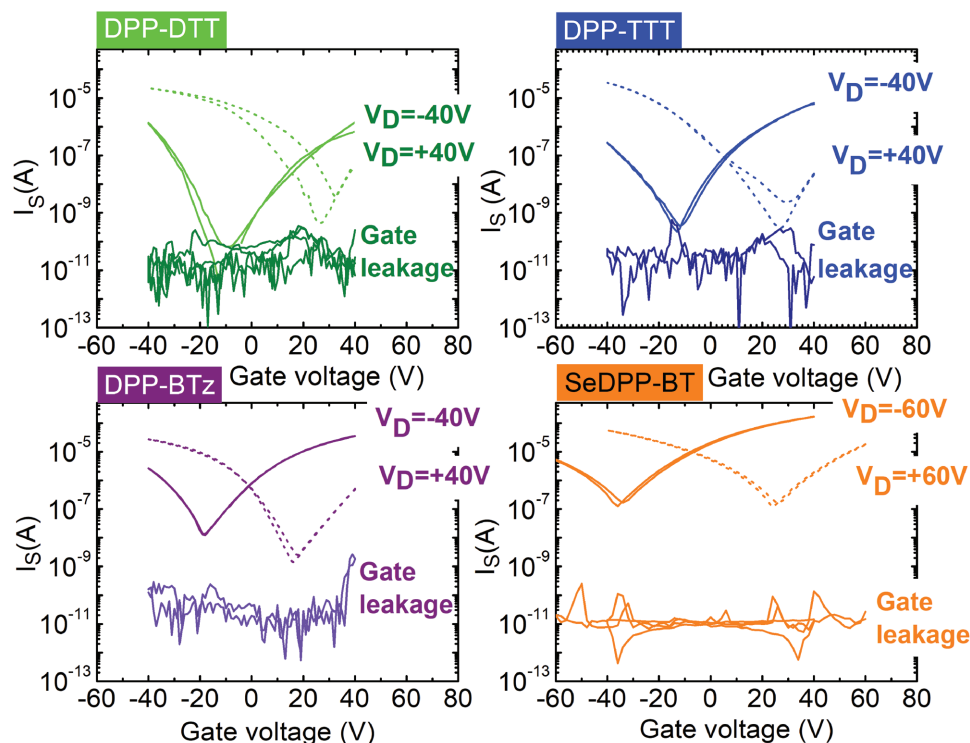


Figure 2. Transfer characteristics of the four different ambipolar polymer devices used for the Seebeck measurements.

and its more amorphous, and potentially less dense microstructure. Note that the values of the Seebeck coefficient for IDTBT reported here are slightly lower than the values reported in ref. [18], which reflects the more accurate measurement of the temperature difference using four-point probe resistance measurements of the temperature sensors used here. Because the DPP copolymers exhibit similarly high charge carrier mobilities than IDTBT, these results suggest that DPP copolymers may be even more suitable for achieving high thermoelectric power factors than IDTBT. However, our results also show that there is only limited scope for optimizing the magnitude of Seebeck coefficient within this family of polymers through molecular design, such as selection of comonomer units.

The magnitudes of the Seebeck coefficient of electrons and holes for a given polymer are very similar within 20%, which reflects the clean ambipolar nature of transport in these materials and is an important finding in the context of thermoelectric applications, as it suggests that in principle n-type and p-type thermoelectric devices could exhibit comparable performance provided, of course, that the electron–hole symmetry

Table 1. Mobilities of electron and holes in ambipolar DPP copolymers.

Organic semiconductor	Hole mobility [cm ² V ⁻¹ s ⁻¹]	Electron mobility [cm ² V ⁻¹ s ⁻¹]	Ref.
DPP-DTT	1.4	1.6	24
DPP-TTT	0.5	0.1	32
DPP-BTz	2.4	1.5	25
SeDPP-BT	0.5	0.8	14
IDTBT	1.5	–	18

observed in our gated Seebeck measurements could be retained in bulk-doped samples.

We now turn to a discussion of the more subtle differences in the carrier concentration dependence of the Seebeck coefficient of the four polymers. In some of the polymers, particularly for holes in SeDPP-BT and DPP-DTT as well as for electrons in DPP-BTz, the Seebeck coefficient exhibits a significantly stronger carrier concentration dependence, that is, the value of $d\alpha/d\log n$ is significantly higher than $k_B/e \ln 10$. For IDTBT, we have shown previously that the carrier concentration dependence is close to what is expected from Heikes formula and this has been interpreted as evidence for the low degree of energetic disorder in IDTBT.^[18] We interpret the stronger carrier concentration dependence in some of the DPP copolymers as evidence for a higher degree of energetic disorder. This is consistent with measurements of the Urbach energy of the optical absorption tail of the polymers. The Urbach energies of the DPP polymers are $E_\mu = 33 \pm 2$ meV (DPP-TTT), 34 ± 2 meV (DPP-BTz), and 39 ± 2 meV (SeDPP-BT) suggesting a higher degree of energetic disorder than in IDTBT which has $E_\mu = 24 \pm 2$ meV. Qualitatively speaking, in the presence of energetic disorder a larger percentage of the charge carriers is trapped at small carrier concentrations and these trapped charges do not contribute to the charge transport. In the presence of significant disorder, the energetic difference between the Fermi level and the energy level at which charge transport occurs increases more strongly with reducing the carrier concentration than in a system with a narrow density of states.

Various transport models for disordered systems have been proposed in the literature, including mobility-edge or

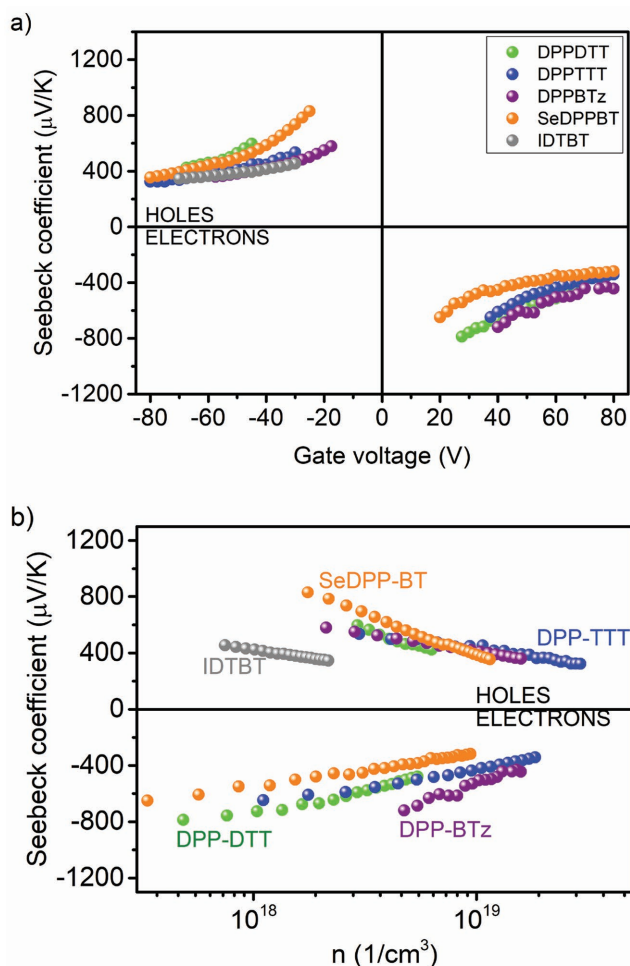


Figure 3. a) Gate voltage and b) charge carrier density dependent Seebeck coefficient for electrons and holes for the various ambipolar polymers studied in this work. IDTBT is shown as reference for a polymer exhibiting low energetic disorder.

hopping-based transport models.^[26–30] All of these models predict a stronger carrier concentration dependence than what is predicted by Heikes formula. These models are applicable primarily to low-mobility polymers in which transport is limited by pronounced energetic disorder, but not to high-mobility, low-disorder polymers such as IDTBT, as was shown previously.^[18] The DPP polymers used here fall somewhere in between; they

Table 2. $\alpha(n)$ measured at high charge carrier densities, and slope of $\alpha(n)$ for the four different DPP polymers studied here. For comparison the values for IDTBT are added.^[18]

Material	Holes		Electrons	
	$\alpha(n)$ [μV K ⁻¹]	Slope of $\alpha(n)$ [μV K ⁻¹ cm ⁻³ decade]	$\alpha(n)$ [μV K ⁻¹]	Slope of $\alpha(n)$ [μV K ⁻¹ cm ⁻³ decade]
DPP-DTT	425	-421	-479	430
DPP-TTT	324	-277	-341	314
DPP-BTz	360	-252	-443	456
SeDPP-BT	353	-591	-318	266
IDTBT	346	-233		

exhibit similarly high carrier mobilities to IDTBT and their energetic disorder is only slightly higher. It is therefore questionable whether variable range or mobility edge models for disordered systems provide appropriate models for the transport in these polymers and for this reason we do not want to make an attempt here to fit the Seebeck data to such models. However, we argue that $d\alpha/d\log n$ provides a qualitative measure of the degree of energetic disorder in these polymers: in systems in which the slope deviates significantly from $k_B/e \ln 10$, that is, holes in SeDPP-BT and DPP-DTT and electrons in DPP-BTz and DPP-DTT, the charge carriers are likely to experience a more disordered energetic environment.

To better understand the nature of energetic disorder in these polymers, we have performed molecular dynamics (MD) simulations combined with density functional theory (DFT) calculations, similar to the simulations for IDTBT performed in ref. [18]. The MD simulations use polymer-adapted reparameterized force fields (see the Experimental Section) to simulate an amorphous phase of the polymer. Although some of the DPP polymers are semicrystalline in thin films, we use amorphous phases for the simulation because they allow us to test the resilience of the polymer backbone conformations and electronic structure to the presence of structural disorder that is inevitably present in solution-processed thin films. Even if such amorphous domains are only at grain boundaries between crystalline domains they may strongly limit the transport properties. The DFT calculations were performed at the B3LYP/6-31G(d,p) level to compute σ_h and σ_e , the width of the energetic disorder relative to the conformational degrees of freedom of the different chains in the film. To complement these we have also performed computations of the effective mass of holes (m_h^*) and electrons (m_e^*) due to the intrachain electronic interactions along the polymer backbone. For this we performed 1D band structure calculations at the B3LYP/6-31G(d,p) level on single polymer chains. These effective mass values provide further insight into the degree of intrachain delocalization of the carrier wavefunction. In a polymer with a smaller effective mass, the charge carriers are more likely to be delocalized along the polymer backbone and are less prone to disorder effects induced by variations in the intermolecular environment. The values for σ and m are summarized in Table 3.

We observe a reasonable correlation between the calculated σ and m values and the FET mobilities. For holes, DPP-BTz and DPP-DTT have values of energetic disorder, σ_h , that are comparable to those of IDTBT suggesting that in these polymers

Table 3. Calculated energetic disorder parameters and effective mass for holes and electrons for the different DPP polymers investigated. For comparison the values for IDTBT are also shown.

Material	Holes		Electrons	
	σ [meV]	m_h^*	σ [meV]	m_e^*
DPP-DTT	56	0.097	61	0.097
DPP-TTT	71	0.119	81	0.111
DPP-BTz	57	0.114	63	0.103
SeDPP-BT	64	0.086	60	0.084
IDTBT	55	0.098		

the electronic structure is similarly resilient to structural disorder as in IDTBT. This is consistent with these two polymers exhibiting the highest hole carrier mobilities among the DPP polymers investigated, with conservatively estimated values exceeding $1 \text{ cm}^2 \text{ V}^{-1} \text{ s}^{-1}$. In contrast, the simulations predict somewhat higher degree of energetic disorder in the HOMO for DPP-TTT and SeDPP-BT, which is consistent with the hole mobilities in these polymers being lower, that is, $<1 \text{ cm}^2 \text{ V}^{-1} \text{ s}^{-1}$. For electrons, we also observe a reasonable correlation between the calculated values of σ_e and m_e with the mobilities of these polymers, for example, DPP-TTT has the highest value of σ_e and largest effective mass, which is consistent with it having the lowest electron mobility.

One observation that may be surprising is that DPP-BTz exhibits such high hole carrier mobilities despite its large effective mass. To understand this better, it is useful to have a closer look at the electronic properties of isolated polymer chains. Interestingly, all DPP copolymers exhibit an unusual frontier molecular orbital localization (Figure 4 and Table S1, Supporting Information) in comparison to common donor-acceptor copolymers such as F8BT.^[31] The HOMO wavefunctions in the DPP copolymers bear dominant contributions on the DPP fragments (>44%), while the LUMO is more delocalized over all subunits. This is opposite to the case of F8BT, where the electron density is confined over the BT units while the hole density spreads out over both electron-poor and electron-rich units. Thus, in DPP-based polymers, we speculate that the propensity to sustain electron wavefunctions extending spatially along the chains is key to reducing disorder. This is borne out by the electron effective masses, m_e^* , calculated on the basis of DFT-optimized geometries: m_e^* is the smallest for SeDPP-BT, the polymer with the smallest σ_e for electrons, and the largest for DPP-TTT, the polymer with the largest σ_e for electrons, following the trend in the calculated and measured values for the energetic disorder. For holes the role of intra-chain delocalization indicated by the value of m_h^* may be less

important to achieve a low degree of energetic disorder as the charges tend to be more localized on the DPP units.

We now turn to a discussion of the comparison between the simulated disorder parameters and the experimental values of $d\alpha/d \log n$. Here, we find a less convincing correlation. Some of the observed Seebeck slopes are as expected from the simulations. For example, for electrons $d\alpha/d \log n$ is lowest for SeDPP-BT and this is consistent with this polymer having the lowest σ_e and m_e . Also the low values of $d\alpha/d \log n$ for holes in DPP-BTz and the high value for holes in SeDPP-BT are qualitatively consistent with the simulated low and high σ_h values, respectively, of these polymers. However, the low values of $d\alpha/d \log n$ for both electrons and holes in DPP-TTT are unexpected, as this polymer should exhibit the highest degree of energetic disorder for both electrons and holes owing to its large values of both σ and m .

For a possible explanation of these discrepancies, we need to consider factors that have so far not been taken into account. As stated above the simulations are performed on amorphous phases of the polymers, whereas there is evidence that the DPP-based polymers used here exhibit significant long-range order and semicrystallinity when annealed.^[14,24,25,32] In semicrystalline polymers, the degree of energetic disorder in the amorphous phases may still be a good predictor of charge carrier mobilities, as there are amorphous grain boundaries between crystalline domains, the energetic disorder in which is likely to limit transport properties. This may explain why we observe a relatively good correlation between the observed mobility values and the simulated disorder parameters. However, the Seebeck coefficient reflects more directly the density of states in the regions where the majority of charges are located and can be expected to be less sensitive to grain boundary effects, if the majority of charge carriers are located in crystalline domains. This may explain why we only observe an imperfect correlation

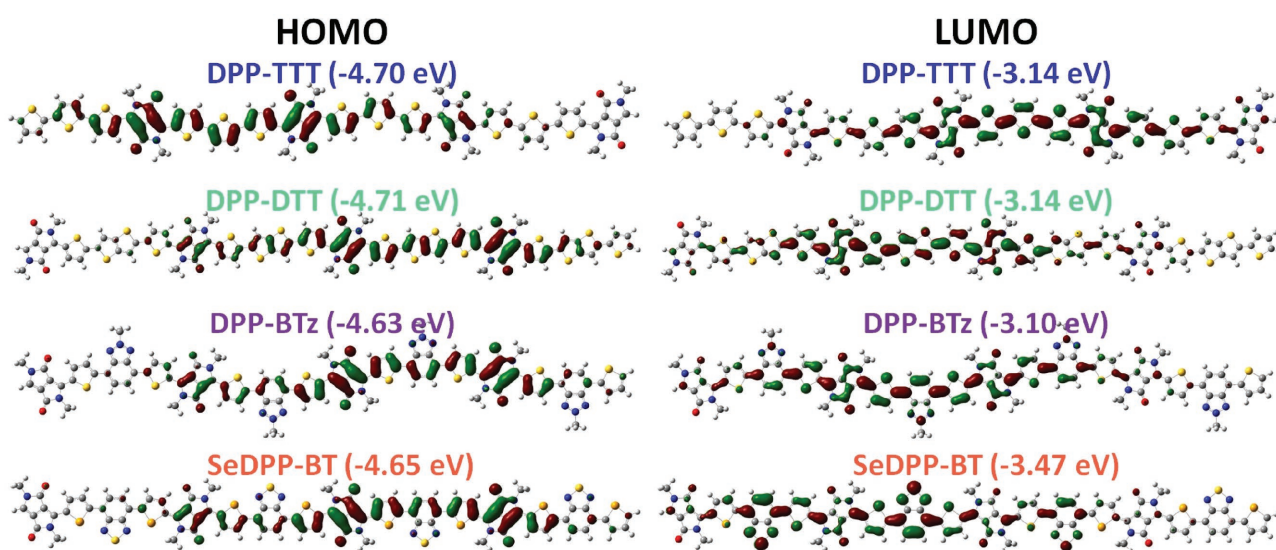


Figure 4. Isocontour plots of the HOMO and LUMO wavefunctions calculated at the DFT (B3LYP/6-31G(d,p)) level on geometry-optimized tetramers of the four DPP-based polymers investigated in this study.

between the Seebeck measurements and the disorder simulations. In a system like DPP-TTT, for which clear semicrystalline order has been reported under the conditions of film formation used here^[32] the presence of crystalline domains may lead to a significant reduction of energetic disorder resulting in a reduction of $d\alpha/d\log n$ that cannot be explained by simulations on amorphous phases. The DPP-based polymers investigated here should planarize when going from the amorphous to the crystalline phase, as demonstrated recently for DPP-DTT.^[33] Reduced torsional disorder in the more crystalline polymers, such as DPP-TTT and DPP-BTZ, is expected to be accompanied by a reduced positional disorder and, as a result, a lower energetic inhomogeneity caused by local variations in electrostatics. This would tend to lower the value of $d\alpha/d\log n$, while it may not be reflected in a high carrier mobility, as long as the charge transport remains limited by grain boundaries. This may explain why DPP-TTT exhibits a small $d\alpha/d\log n$ that is not accompanied by a high charge carrier mobility.

A further factor that has not yet been taken into account is a potential preferential orientation of the polymer with respect to the substrate. DPP-BTZ shows predominantly face-on orientation^[25] and DPP-TTT as well as SeDPP-BT have been reported to exhibit at least partial face-on orientation at the interface to the electrodes.^[14,32] DPP-DTT is the only polymer of these four semicrystalline materials for which a pronounced edge-on orientation and no indication of face-on orientation have been found.^[24] It is possible that the relatively large $d\alpha/d\log n$ for this polymer is related to the edge-on orientation of the polymer, as in edge-on oriented domains the energetic disorder may be more sensitive to disorder in the π - π stacking distances along the interface than in face-on oriented domains, because in the latter the number of adjacent chains along the π - π stacking direction is constrained by the thickness of the accumulation layer.

In principle, it is possible to take into account in the simulations effects of crystallinity and molecular orientation with respect to the substrate,^[34] but this goes significantly beyond the scope of the present paper. What is clear from the present simulations, however, is that the two highest mobility DPP polymers considered here, DPP-DTT and DPP-BTZ, owe their excellent charge transport properties to a similarly low degree of energetic disorder as is present in IDTBT.

3. Conclusions

In conclusion, we have reported for the first time measurements of the Seebeck coefficients for electrons and holes in high-mobility ambipolar DPP copolymers. Our results demonstrate that the technique of carrier-modulated Seebeck measurements is well suited to investigate the relationship between molecular structure and Seebeck coefficient. At high carrier concentrations where trapping effects are less important we find Seebeck coefficients of very similar magnitude in these polymers suggesting that the Seebeck coefficient is not strongly dependent on the molecular structure of the backbone within

this family of polymers. Also the Seebeck coefficients of electrons and holes have very similar magnitudes showing that electrons and holes experience a similar energetic landscape. However, there are subtle differences in the carrier concentration dependence between the polymers and our results suggest that these are related to differences in the energetic disorder in these polymers with higher energetic disorder resulting in a more pronounced carrier concentration. Our results also provide further evidence that low energetic disorder for holes and electrons leads to high charge carrier mobility, not only in near-amorphous polymers like IDTBT, but also in semicrystalline DPP copolymers. Finally, our observation of a similar magnitude for the Seebeck coefficient of electrons and holes shows that it should be possible to realize both p- and n-type organic thermoelectric materials with comparable thermoelectric performance, provided that suitable bulk doping methods can be developed.

4. Experimental Section

Device Fabrication: The devices used in this work for the measurement of the Seebeck coefficient and transistor characteristics were fabricated on glass substrates using a multistep photolithography procedure. First, source-drain electrodes and an on-chip stripe heater made from evaporated Au (20 nm) were fabricated on glass substrates using photolithography. An interlayer of Cr (5 nm) was used to enhance adhesion of Au on glass. In the architecture used, a heater is positioned 20 μm away from one of the electrodes and the channel length between the source and drain electrodes was 50 μm . The ambipolar polymer (50 nm thick) was solution processed over these electrodes in a N_2 glove box from a solution of 10 mg dissolved in 1 mL dichlorobenzene. The organic semiconductor was then patterned into a rectangular shape of 1 mm \times 100 μm in such a way that it did not overlap with the heater, thus avoiding electrical crosstalk between the on-chip heater and the organic semiconductor during a thermal voltage/Seebeck measurement. The procedure of patterning the organic semiconductor on the chip involves a second step of photolithography and has been described and used in earlier work.^[17,18] A 300 nm layer of PMMA was then spin-coated onto the substrates containing the patterned organic semiconductor and baked at 80 $^\circ\text{C}$ for 30 min. Finally, an aluminium metal top gate (30 nm) electrode was thermally evaporated onto the dielectric through a shadow mask.

Measurement of the Seebeck Coefficient and Transistor Characteristics: The thermal voltage (from which the Seebeck coefficient was estimated) as well as the transistor transfer characteristics were measured using an Agilent semiconductor parameter analyser 4155B using high input impedance source measure units. To estimate the Seebeck coefficient, the temperature gradient between the source and drain electrodes was estimated by measuring the resistance increase of the two resistance thermometers (source and drain electrodes) as a function of the heater power applied. The change in resistance with heater power of each individual resistance thermometer was then converted into a temperature using the temperature coefficient of resistance of each thermometer, a quantity that is measured separately. The difference between the two estimated temperatures at the hot and the cold ends of the patterned organic yields the temperature difference across the organic semiconductor. The measured thermal voltage across the organic semiconductor for a given heater power is plotted against the temperature difference for the same heater power, and the slope of several such data points with different heater power yields an estimate of the Seebeck coefficient. An upper limit on the measurement error in the Seebeck coefficient achieved by propagating the errors in each measurement is 10%.

Simulations: To simulate the energetic disorder within an amorphous phase, molecular dynamics simulations were first performed on systems containing 24 oligomers of DPP derivatives made of ten repeating units that are replicated in all directions. All molecular mechanics/dynamics calculations were performed within the Materials Studio (MS) 6.0 package^[35] using force-fields derived from the Dreiding force-field in which inter-subunit torsion potentials as well as torsions between the conjugated cores and alkyl chains were reparameterized against reference DFT calculations using the B3LYP functional and the cc-pvtz basis set.^[36–38] The atomic charges were obtained by fitting the electrostatic potential (ESP charges^[39]) calculated at the B3LYP/cc-pvtz level on an isolated dimer.

The procedure to generate these amorphous systems is the following: (i) 24 oligomers have been put randomly in a large unit cell (300 Å × 300 Å × 300 Å) and subject to a 500 ps high-temperature molecular dynamics (NVT; $T = 1000$ K) while keeping the density low (≈ 0.02 g cm⁻³) to favor random distribution of the oligomers; (ii) five successive 500 ps molecular dynamics (NPT, $P = 1$ atm) were then performed at decreasing temperature (1000, 500, 400, 350, 300 K); (iii) finally, a 2 ns molecular dynamics (NPT; $P = 1$ atm, $T = 300$ K) was performed and snapshots saved every 5 ps for further analysis.

The electronic properties of each system were characterized by computing the electronic structure of isolated polymer chains, namely, DPP octamers, extracted from the amorphous phase at the DFT level using the B3LYP functional and the 6-31G(d,p) basis set. The calculations were performed over 100 snapshots, equally distributed over the 2 ns molecular dynamics runs, of ten randomly selected oligomers. To quantify the impact of the structural disorder on the electronic behavior of each system, the energetic disorder parameter σ relative to hole (electron) transport is estimated as the standard deviation of the computed HOMO (LUMO) energies.

The efficiency of intramolecular charge transport within the amorphous phase was characterized by evaluating the hole and electron effective mass as extracted from electronic bandwidths calculations for model systems at the DFT level using the B3LYP functional and the 6-31G(d,p) basis set. These model systems consist of single chains containing two monomer units which are replicated in one direction to mimic infinite isolated polymer chains. These dimers are extracted from the central monomer units of DFT (B3LYP/6-31G(d,p))-optimized tetramers.

Supporting Information

Supporting Information is available from the Wiley Online Library or from the author.

Acknowledgements

The authors gratefully acknowledge financial support from the European Research Council (ERC) through a synergy grant (No. 610115) and the Engineering and Physical Sciences Research Council (EPSRC). The work in the Laboratory for Chemistry of Novel Materials was supported by the European Commission/Région Wallonne (FEDER – BIORGEL project), the Interuniversity Attraction Pole program of the Belgian Federal Science Policy Office (PAI 7/05), the Programme d'Excellence de la Région Wallonne (OPTI2MAT project), the Consortium des Équipements de Calcul Intensif (CÉCI), funded by the Fonds de la Recherche Scientifique de Belgique (F.R.S.-FNRS) under Grant No. 2.5020.11, and FRS-FNRS, the European Unions Horizon 2020 research and innovation program under Grant Agreement No. 646176 (EXTMOS project). D.B. is an FNRS Research Director. K.B. gratefully acknowledges financial support from the German Research Foundation (BR 4869/1-1) and the Institutional Strategy of the University of Tuebingen (Deutsche Forschungsgemeinschaft ZUK63).

Conflict of Interest

The authors declare no conflict of interest.

Keywords

ambipolar transport, organic semiconductors, organic thermoelectrics, Seebeck coefficient

Received: May 29, 2017

Revised: July 25, 2017

Published online: August 23, 2017

- [1] Q. Zhang, Y. Sun, W. Xu, D. Zhu, *Adv. Mater.* **2014**, *26*, 6829.
- [2] Y. Chen, Y. Zhao, Z. Liang, *Energy Environ. Sci.* **2015**, *8*, 401.
- [3] H. B. Callen, *Thermodynamics*, John Wiley & Sons, New York **1960**.
- [4] D. Emin, *Polarons*, Cambridge University Press, New York **2012**.
- [5] G. S. Nolas, J. Sharp, J. Goldsmid, *Thermoelectrics: Basic Principles and New Materials Developments*, Springer, New York **2001**.
- [6] A. Shakouri, *Annu. Rev. Mater. Res.* **2011**, *41*, 399.
- [7] D. M. Rowe, *Thermoelectrics Handbook: Macro to Nano*, CRC Press Taylor and Francis Group, Boca Raton, FL **2006**.
- [8] C. J. Vineis, A. Shakouri, A. Majumdar, M. G. Kanatzidis, *Adv. Mater.* **2010**, *22*, 3970.
- [9] K. Biswas, J. He, I. D. Blum, C.-I. Wu, T.P. Hogan, D. N. Seidman, V. P. Dravid, M. G. Kanatzidis, *Nature* **2012**, *489*, 414.
- [10] B. Poudel, Q. Hao, Y. Ma, Y. Lan, A. Minnich, B. Yu, X. Yan, D. Wang, A. Muto, D. Vashaee, X. Chen, J. Liu, M. S. Dresselhaus, G. Chen, Z. Ren, *Science* **2008**, *320*, 634.
- [11] G.-H. Kim, L. Shao, K. Zhang, K. P. Pipe, *Nat. Mater.* **2013**, *12*, 719.
- [12] O. Bubnova, Z. U. Khan, A. Malti, S. Braun, M. Fahlman, M. Berggren, X. Crispin, *Nat. Mater.* **2011**, *10*, 429.
- [13] D. A. Mengistie, C.-H. Chen, K. M. Boopathi, F. W. Pranoto, L.-J. Li, C.-W. Chu, *Appl. Mater. Interfaces* **2015**, *7*, 94.
- [14] A. J. Kronemeijer, E. Gili, M. Shahid, J. Rivnay, A. Salleo, M. Heeney, H. Sirringhaus, *Adv. Mater.* **2012**, *24*, 1558.
- [15] A. J. Kronemeijer, V. Pecunia, D. Venkateshvaran, M. Nikolka, A. Sadhanala, J. Moriarty, M. Szumilo, H. Sirringhaus, *Adv. Mater.* **2014**, *26*, 728.
- [16] J. Li, Y. Zhao, H. S. Tan, Y. Guo, C.-A. Di, G. Yu, Y. Liu, M. Lin, S. H. Lim, Y. Zhou, H. Su, B. S. Ong, *Sci. Rep.* **2012**, *2*, 754.
- [17] D. Venkateshvaran, A. J. Kronemeijer, J. Moriarty, D. Emin, H. Sirringhaus, *APL Mater.* **2014**, *2*, 032102.
- [18] D. Venkateshvaran, M. Nikolka, A. Sadhanala, V. Lemaury, M. Zelazny, M. Kepa, M. Hurhangee, A. J. Kronemeijer, V. Pecunia, I. Nasrallah, I. Romanov, K. Broch, I. McCulloch, D. Emin, Y. Olivier, J. Cornil, D. Beljonne, H. Sirringhaus, *Nature* **2014**, *515*, 384.
- [19] K. P. Pernstich, B. Rössner, B. Batlogg, *Nat. Mater.* **2008**, *7*, 321.
- [20] W. C. Germs, K. Guo, R. A. J. Janssen, M. Kemerink, *Phys. Rev. Lett.* **2012**, *109*, 016601.
- [21] F. Zhang, Y. Zang, D. Huang, C.-A. Di, X. Gao, H. Sirringhaus, D. Zhu, *Adv. Funct. Mater.* **2015**, *25*, 3004.
- [22] C. N. Warwick, D. Venkateshvaran, H. Sirringhaus, *APL Mater.* **2015**, *3D*, 096104.
- [23] D. Emin, *Wiley Encyclopedia of Electrical and Electronics Engineering Online*, John Wiley and Son, New York **2014**.
- [24] Z. Chen, M. J. Lee, R. S. Ashraf, Y. Gu, S. A. Seifried, M. M. Nielsen, B. Schroeder, T. D. Anthopoulos, M. Heeney, I. McCulloch, H. Sirringhaus, *Adv. Mater.* **2012**, *24*, 647.
- [25] M. Gruber, S.-H. Jung, S. Schott, D. Venkateshvaran, A. J. Kronemeijer, J. W. Andreasen, C. R. McNeill, W. W. H. Wong,

- M. Shahid, M. Heeney, J.-K. Lee, H. Sirringhaus, *Chem. Sci.* **2015**, *6*, 6949.
- [26] J. J. Brondijk, W. S. C. Roelofs, S. G. J. Mathijssen, A. Shehu, T. Cramer, F. Biscarini, P. W. M. Blom, D. M. de Leeuw, *Phys. Rev. Lett.* **2012**, *109*, 056601.
- [27] G. Zuo, H. Abdalla, M. Kemerink, *Phys. Rev. B* **2016**, *93*, 235203.
- [28] M. C. J. M. Vissenberg, M. Matters, *Phys. Rev. B* **1998**, *57*, 12964.
- [29] R. Schmechel, *J. Appl. Phys.* **2003**, *93*, 4653.
- [30] G. Kim, K. P. Pipe, *Phys. Rev. B* **2012**, *86*, 085208.
- [31] J. Cornil, I. Gueli, A. Dkhissi, J. C. Sancho-Garcia, E. Hennebicq, J. P. Calbert, V. Lemaury, D. Beljonne, J. L. Brédas, *J. Chem. Phys.* **2003**, *118*, 6615.
- [32] X. Zhang, L. J. Richter, D. M. DeLongchamp, R. J. Kline, M. R. Hammond, I. McCulloch, M. Heeney, R. S. Ashraf, J. N. Smith, T. D. Anthopoulos, B. Schroeder, Y. H. Geerts, D. A. Fischer, M. F. Toney, *J. Am. Chem. Soc.* **2011**, *133*, 15073.
- [33] S. R. Chaudhari, J. M. Griffin, K. Broch, A. Lesage, V. Lemaury, D. Dudenko, Y. Olivier, H. Sirringhaus, L. Emsley, C. P. Grey, *Chem. Sci.* **2017**, *8*, 3126.
- [34] N. G. Martinelli, M. Savini, L. Muccioli, Y. Olivier, F. Castet, C. Zannoni, D. Beljonne, J. Cornil, *Adv. Funct. Mater.* **2009**, *19*, 3254.
- [35] MS Modelling v6.0.0.0, Accelrys Software Inc., San Diego, CA **2011**.
- [36] S. L. Mayo, B. D. Olafson, W. A. Goddard, *J. Phys. Chem.* **1990**, *94*, 8897.
- [37] V. Lemaury, L. Muccioli, C. Zannoni, D. Beljonne, R. Lazzaroni, J. Cornil, Y. Olivier, *Macromolecules* **2013**, *46*, 8171.
- [38] Y. Olivier, D. Niedzialek, V. Lemaury, W. Pisula, K. Müllen, U. Koldemir, J. R. Reynolds, R. Lazzaroni, J. Cornil, D. Beljonne, *Adv. Mater.* **2014**, *26*, 2119.
- [39] B. H. Besler, K. M. Merz, P. A. Kollman, *J. Comput. Chem.* **1990**, *11*, 431.